SCIENCE CHINA Materials ARTICLES

mater.scichina.com link.springer.com

Published online 2 September 2020 | https://doi.org/10.1007/s40843-020-1462-4
Sci China Mater 2020, 63(12): 2487–2496

Phase degradation of all-inorganic perovskite $CsPbI_2Br$ films induced by a p-type CuI granular capping layer

Zhi Zhu[1,2], Wenjing Su[1,2], Jianyong Feng[1,3,4,5], Jincheng Li[1,2], Xiaopeng Han[1,2], Tao Yu[1,2,3,4*], Zhaosheng Li[1,3,4,5] and Zhigang Zou[1,2,3,4]

ABSTRACT **It is necessary to evaluate the interactions between the different functional layers in optoelectronic devices to optimize device performance. Recently, the I-rich all-inorganic perovskite $CsPbI_2Br$ has attracted tremendous attention for use in solar cell applications because of its suitable band gap and favorable photo and thermal stabilities. It has been reported that the undesirable phase degradation of the photoactive α phase $CsPbI_2Br$ to the non-perovskite δ phase could be triggered by high humidity. To obtain stable devices, it is thus important to protect $CsPbI_2Br$ from moisture. In this paper, CuI, a non-hygroscopic p-type hole-transporting material, is found to induce the phase degradation of α-$CsPbI_2Br$ to the δ-$CsPbI_2Br$. The rate and extent of phase degradation of $CsPbI_2Br$ are closely associated with the heating temperature and coverage of a CuI granular capping layer. This discovery is different from the widely reported water-induced phase degradation of $CsPbI_2Br$. Our work highlights the importance of careful selection of hole-transporting materials during the processing of I-rich all-inorganic $CsPbX_3$ (X=Br, I) perovskites to realize high-performance optoelectronic devices.**

Keywords: $CsPbI_2Br$, CuI, phase degradation, perovskite, hole-transporting material

INTRODUCTION

Recently, research on inorganic perovskite solar cells (PSCs) based on $CsPbI_xBr_{3-x}$ has been progressing rapidly [1–6]. Among known light-absorbing materials, $CsPbI_2Br$ has attracted wide attention from researchers [7–9] because of its narrow band gap [10,11], high theoretical power conversion efficiency (PCE) [12], good photo and thermal stabilities, and suitable tolerance factor [13,14]. However, $CsPbI_2Br$ is sensitive to humidity. The photoactive α phase of $CsPbI_2Br$ (α-$CsPbI_2Br$, black phase) easily converts to the non-perovskite δ phase (δ-$CsPbI_2Br$, yellow phase) under high humidity [15–18].

It is essential to establish a suitable physical barrier between α-$CsPbI_2Br$ and moisture to improve the stability of α-$CsPbI_2Br$-based devices in the atmosphere. Moreover, inadvertent introduction of water in other layers of PSCs can induce phase degradation of $CsPbI_2Br$ during device fabrication. Previous study revealed that $CsPbI_2Br$ PSCs using doped 2,2′,7,7′-tetrakis(*N*,*N*-di-*p*-methoxyphenylamine)-9,9′-spirobifluorene (Spiro-OMeTAD) as a hole-transporting material (HTM) showed much lower stability than that of a pure $CsPbI_2Br$ film under the same conditions [16]. Further studies indicated that the lithium salt contained in Spiro-OMeTAD is hygroscopic, which exacerbates device instability [16,19–22]. Therefore, water should be excluded from the whole device fabrication process, including the introduction of the charge-transporting layer, to avoid the undesired phase degradation of α-$CsPbI_2Br$.

Dopants such as lithium salts have been widely introduced into organic HTMs to improve their hole mobility. However, most of these additives are hygroscopic [21–23]. Therefore, inorganic HTMs may have advantages over their organic counterparts for assembling PSCs based on $CsPbI_2Br$ [24–29]. Among all the candidate inorganic HTMs, CuI has received extensive atten-

[1] National Laboratory of Solid State Microstructures, Nanjing University, Nanjing 210093, China
[2] Ecomaterials and Renewable Energy Research Center (ERERC), School of Physics, Nanjing University, Nanjing 210093, China
[3] Collaborative Innovation Center of Advanced Microstructures, Nanjing University, Nanjing 210093, China
[4] Jiangsu Provincial Key Laboratory for Nanotechnology, Nanjing University, Nanjing 210093, China
[5] College of Engineering and Applied Sciences, Nanjing University, Nanjing 210093, China
* Corresponding author (email: yutao@nju.edu.cn)

tion because of its wide band gap, high hole mobility [30–33], acceptable stability [34,35], and low cost [36–38]. Most importantly, CuI is non-hygroscopic [39–42]. In this study, we fabricate devices containing CuI as an HTM. Unexpectedly, after the CuI precursor is spin-coated on the $CsPbI_2Br$ film and heated, the film color changes from black to yellow. This color change generally represents a transition from α-$CsPbI_2Br$ to δ-$CsPbI_2Br$, which is confirmed by X-ray diffraction (XRD) and light absorption measurements. Further investigation of this phase transformation process suggests that it is related to the presence of a CuI granular capping layer. Moreover, the rate and extent of phase degradation of $CsPbI_2Br$ depend on both the heating temperature and coverage of the CuI granular capping layer. This paper reveals that CuI—a substance other than water—can induce the phase degradation of α-$CsPbI_2Br$. Therefore, special caution is needed when selecting inorganic HTMs for use with I-rich $CsPbX_3$(X=Br, I) perovskites in high-performance optoelectronic devices.

EXPERIMENTAL SECTION

The conductive surface of the FTO (SnO_2:F) glass substrate was first cleaned with detergent. The FTO substrate was then ultrasonically cleaned sequentially with deionized water, acetone, and ethanol for 20 min each, followed by drying under a nitrogen (N_2) stream. A compact TiO_2 (c-TiO_2) layer was deposited on the cleaned FTO glass substrate and then annealed at 480°C for 40 min.

The $CsPbI_2Br$ film was formed by one-step spin coating. First, PbI_2 (0.277 g), $PbBr_2$ (0.220 g), and CsI (0.312 g) were dissolved in dimethyl sulfoxide (DMSO, 1 mL). The mixture was stirred at 60°C in an N_2-filled glove box until a clear solution was obtained. The $CsPbI_2Br$ precursor solution was dropped onto the TiO_2 substrate and then spin-coated *via* a two-step process (1500 rpm for 10 s and then 5000 rpm for 30 s). The film annealing process also entailed two steps. After spin coating, the device was placed on a hot plate at 42°C for about 1 min to form a brown film. Subsequently, the device was placed on a hot plate at 160°C for 10 min to evaporate the solvents and provide an α-$CsPbI_2Br$ film [11].

A CuI granular layer was also prepared by spin coating. CuI (0.019 g) was added to a mixture of dipropyl sulfide and chlorobenzene (1 mL, 1:39 *v*/*v*). The mixture was stirred until it became clear, which indicated the formation of CuI colloids [43]. The CuI colloid solution was spin coated on the $CsPbI_2Br$ film at 4000 rpm for 30 s and then annealed.

XRD patterns were collected on a Rigaku Ultima III X-ray diffractometer using Cu-Kα radiation. A Varian Cary-50 spectrophotometer was used to measure the absorption properties of the samples. Photoluminescence (PL) spectra were collected at room temperature on a fluorescence spectrophotometer with an excitation wavelength of 405 nm. X-ray photoemission spectroscopy (XPS) analysis was conducted on a Thermo Scientific K-Alpha photoelectron spectrometer. A Zeiss GeminiSEM 500 ultra-high-resolution scanning electron microscope equipped with an Oxford energy-dispersive X-ray spectroscopy (EDS) system was used to characterize the morphological properties of the samples.

RESULTS AND DISCUSSION

A device with a structure of FTO/TiO_2/$CsPbI_2Br$/CuI was prepared in an N_2-filled glove box to avoid water contamination. Fig. 1 shows the fabrication process of this device. The scanning electron microscopy (SEM) image (Fig. S1) reveals that the device contained a smooth and dense $CsPbI_2Br$ film. The device was thermally annealed to increase the density of the hole-transporting layer (HTL) and improve its contact with the light-absorbing layer. In addition, the solvent was completely evaporated during annealing [44–48]. However, it was unexpectedly found that the film color converted from black to yellow during thermal annealing. This color change process only took several minutes when the device was heated at 160°C. Therefore, a heating temperature of 160°C was initially chosen to facilitate our exploration of this phenomenon. According to previous reports, such a color change is related to the phase transition of α-$CsPbI_2Br$ to δ-$CsPbI_2Br$.

Although CuI itself does not absorb water, it is possible that moisture may accumulate in the CuI sample during storage. To investigate whether the observed color change is associated with the interference of moisture, the CuI powder was heated under an N_2 atmosphere at 200°C for 30 min. The CuI colloid formed by dissolving CuI powder in a mixture of dipropyl sulfide and chlorobenzene with a volume ratio of 1:39 was then spin coated on the $CsPbI_2Br$ film, followed by annealing at 160°C for 10 min. However, the color change still occurred (Photograph 1 in Fig. 2a). This result confirmed that the color change did not arise from water. Ultraviolet–visible (UV-vis) spectra of the CuI-coated $CsPbI_2Br$ and pure black $CsPbI_2Br$ are shown in Fig. 2b. The optical absorption edge of the pure black $CsPbI_2Br$ is at about 670 nm, which is the characteristic absorbance of the α phase. However, this characteristic α-phase absorbance dis-

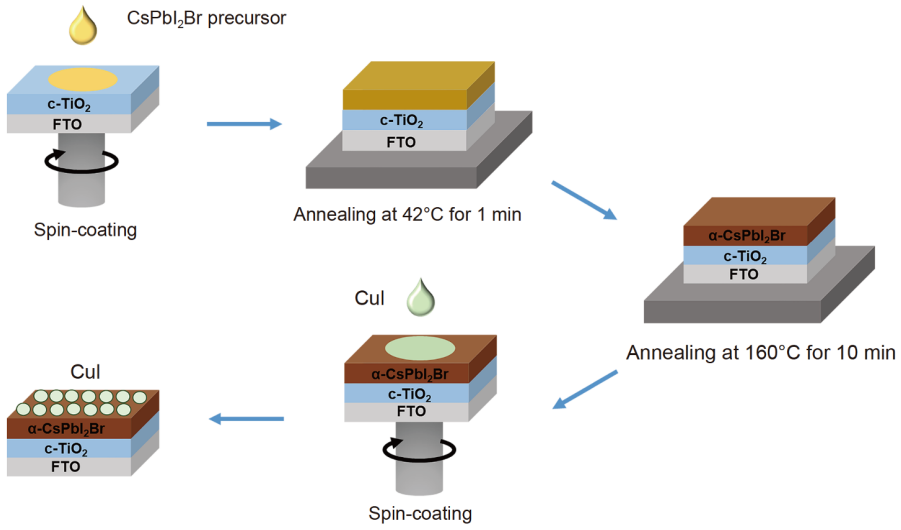

Figure 1 Schematic of the fabrication process of a device with a structure of FTO/TiO_2/$CsPbI_2Br$/CuI in an N_2-filled glove box.

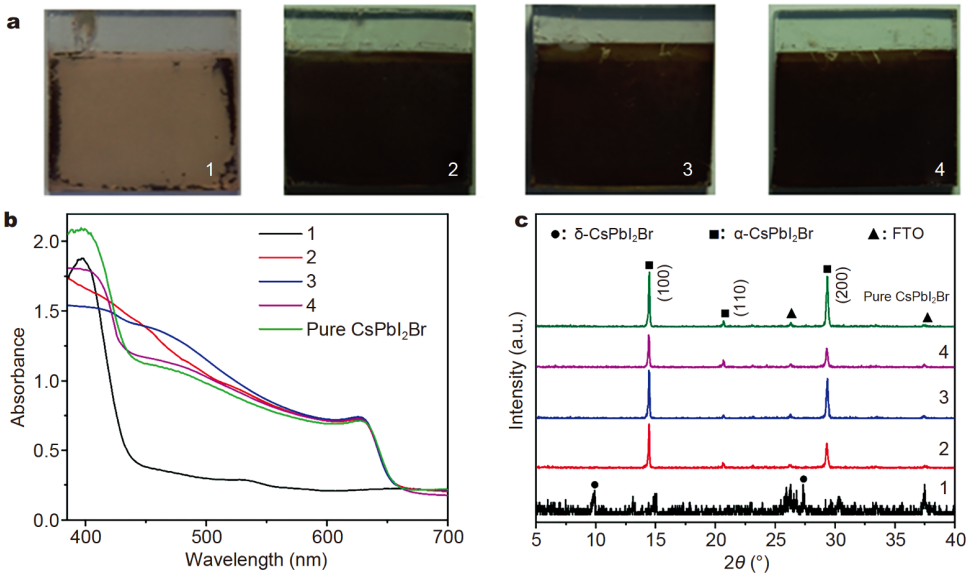

Figure 2 (a) Photographs, (b) UV-vis spectra, and (c) XRD patterns of the $CsPbI_2Br$ films covered with (1) water-removal CuI colloids, (2) solvent mixture, (3) dipropyl sulfide, and (4) chlorobenzene (heated at 160°C).

appeared for the devices covered with CuI. Meanwhile, the absorption edge of δ-$CsPbI_2Br$ at about 450 nm was observed [15]. The XRD pattern of the CuI-coated $CsPbI_2Br$ film, which is shown in Fig. 2c, indicated that the film transformed to δ-$CsPbI_2Br$ [15]. In addition, there are no peaks from other possible reaction products such as PbI_2, which reveals that the observed color change is caused by the α-to-δ phase transition of $CsPbI_2Br$, not a chemical reaction with CuI or the decomposition of $CsPbI_2Br$.

It is important to investigate whether the solvent of CuI could induce the phase transition of the $CsPbI_2Br$ film. Dipropyl sulfide, chlorobenzene, and a mixture of them with a volume ratio of 1:39 were spin coated on $CsPbI_2Br$ films, followed by annealing. Photographs 2–4 in Fig. 2a show that all the solvent-treated films remained black after heating. The UV-vis spectra in Fig. 2b and XRD patterns in Fig. 2c indicate that there is no obvious difference between the pure α-$CsPbI_2Br$ film and the films after treatment with the solvents described above. These

results verified that the phase transition was independent of the solvent of CuI. The photographs, UV-vis spectra, and XRD patterns illustrate that the phase transition of α-$CsPbI_2Br$ to δ phase occurs during annealing for the sample with the CuI granular capping layer. Therefore, this process is different from the widely recognized water-induced phase degradation of $CsPbI_2Br$.

The conditions under which the CuI granular capping layer induces this α-to-δ phase transition in $CsPbI_2Br$ were then explored. Because this transition occurs during annealing, it is essential to investigate the effect of heating temperature on this phase transition. FTO/TiO_2/$CsPbI_2Br$/CuI devices were fabricated and heated at 80, 120, 160, and 200°C for 10 min, respectively. The photographs in Fig. 3a reveal that the film color changed more obviously with increasing temperature. Fig. 3b shows the UV-vis spectra of the above four devices. Compared with that of pure α-$CsPbI_2Br$, the intensity of the characteristic α-phase absorption of the above four devices decreased. When the annealing temperature was 160°C or higher, the characteristic absorbance of α-$CsPbI_2Br$ disappeared, corresponding to the nearly complete color change and phase transition of the films. Fig. 3c shows the XRD patterns of the above four devices. The intensity of the α-phase peaks decayed rapidly at above 120°C and the α-phase peaks had almost disappeared at 200°C. Correspondingly, the δ-phase peaks became more obvious at higher temperature. The above results indicate that the rate of the α-to-δ phase transition in $CsPbI_2Br$ is temperature-dependent. The higher the annealing temperature, the faster the phase transformation. Fig. 3d presents a schematic of the $CsPbI_2Br$ phase degradation induced by the CuI granular capping layer at different temperatures.

Steady-state PL measurements were conducted on pure $CsPbI_2Br$, CuI-coated $CsPbI_2Br$ (at room temperature, RT), and CuI-coated $CsPbI_2Br$ heated at 160°C to investigate the influence of CuI on $CsPbI_2Br$. As shown in Fig. 4a, the black pure $CsPbI_2Br$ and CuI-coated $CsPbI_2Br$ (RT) films exhibited emission peaks at ~650 nm, in good agreement with the band gap of α-$CsPbI_2Br$ [7]. Therefore, the presence of CuI does not induce an obvious phase transition of α-$CsPbI_2Br$ without heating. The sharply decreased PL intensity of CuI-coated $CsPbI_2Br$ (RT) compared with that of pure α-$CsPbI_2Br$ can be explained by the hole transport ability of CuI in the former sample. In contrast, the characteristic peak at ~650 nm for α-$CsPbI_2Br$ almost disappeared for the CuI-coated

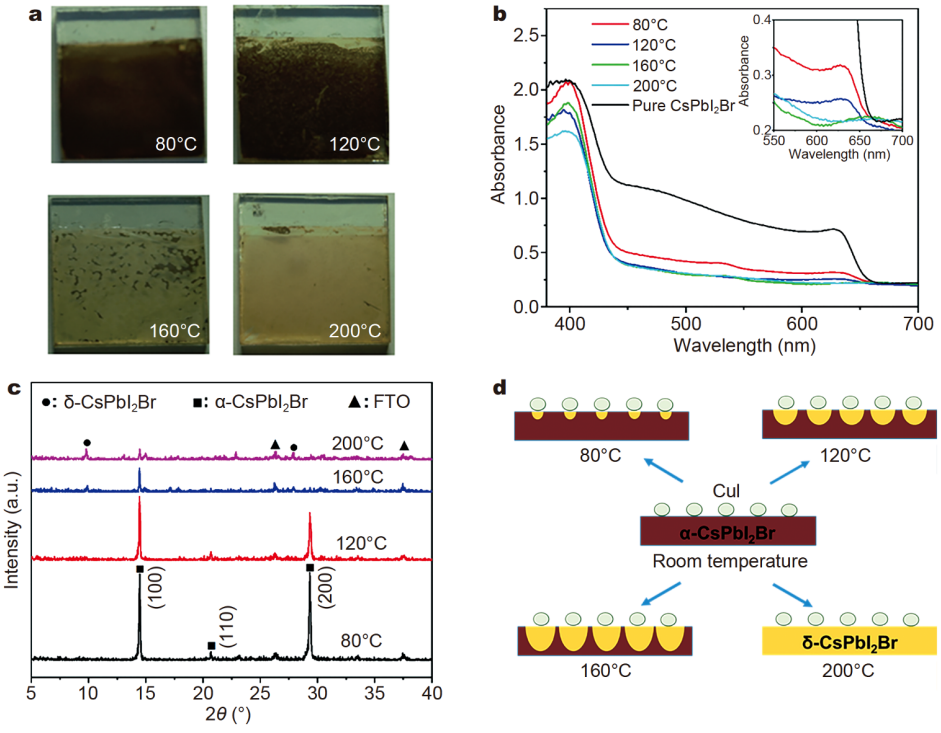

Figure 3 (a) Photographs, (b) UV-vis spectra, and (c) XRD patterns of the $CsPbI_2Br$ films covered with CuI colloidal particles and heated at different temperatures for 10 min. (d) Schematic of the $CsPbI_2Br$ phase degradation induced by the CuI granular capping layer heated at different temperatures.

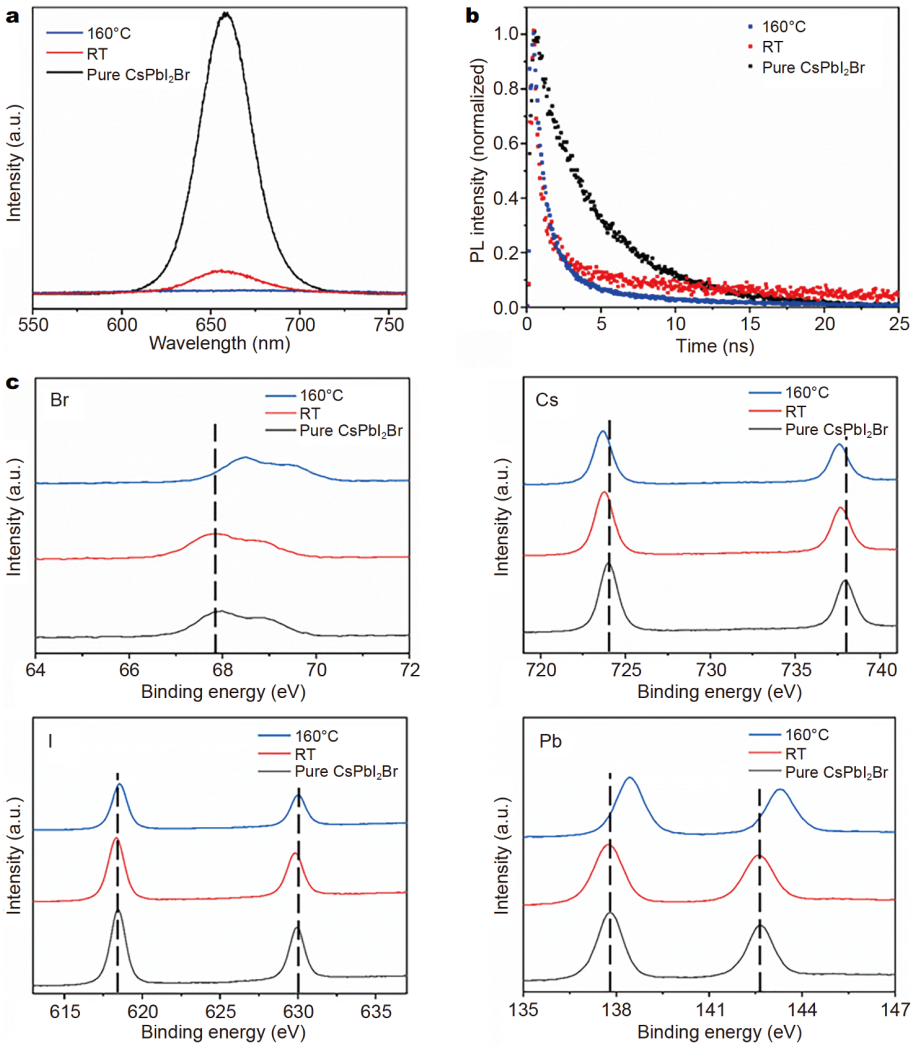

Figure 4 (a) Steady-state PL spectra and (b) TRPL spectra of pure $CsPbI_2Br$, CuI-coated $CsPbI_2Br$ (RT), and CuI-coated $CsPbI_2Br$ heated at 160°C. (c) XPS analyses of Cs, Pb, Br, and I in pure $CsPbI_2Br$, CuI-coated $CsPbI_2Br$ (RT), and CuI-coated $CsPbI_2Br$ heated at 160°C.

$CsPbI_2Br$ film heated at 160°C, which is consistent with the α-to-δ phase transition of $CsPbI_2Br$ indicated by the XRD results.

The time-resolved PL (TRPL) decay spectra of the three samples are shown in Fig. 4b. The decay curves were fitted by a biexponential equation:

$$\tau = A_1\exp(-t/\tau_1) + A_2\exp(-t/\tau_2), \quad (1)$$

where τ_1 and τ_2 are slow and fast decay time constants, respectively, and A_1 and A_2 are the corresponding fractional amplitudes of τ_1 and τ_2, respectively. The fast decay of PL intensity is related to defect-induced nonradiative recombination, whereas the slow component is caused by radiative recombination. The TRPL parameters of pure $CsPbI_2Br$, CuI-coated $CsPbI_2Br$ (RT), and CuI-coated $CsPbI_2Br$ heated at 160°C are summarized in Table 1. The calculated average PL decay lifetime (τ) for the pure $CsPbI_2Br$ film is 6.67 ns, whereas those of the CuI-coated film (RT) and CuI-coated film heated at 160°C exhibited τ of 4.32 and 2.78 ns, respectively. The shorter PL lifetime of CuI-coated $CsPbI_2Br$ (RT) than that of pure $CsPbI_2Br$ is related to the hole transport ability of CuI, as discussed above. Meanwhile, the decreased PL lifetime of the CuI-coated $CsPbI_2Br$ film after heating at 160°C is obviously induced by the phase degradation of $CsPbI_2Br$. To summarize, both PL and TRPL data demonstrated that after application of CuI and heating at high temperatures, the original perovskite structure of α-$CsPbI_2Br$ was converted to the non-photoactive δ phase.

Next, XPS measurements were carried out for pure $CsPbI_2Br$, CuI-coated $CsPbI_2Br$ (RT), and CuI-coated

Table 1 Parameters of the TRPL spectra for pure $CsPbI_2Br$, CuI-coated $CsPbI_2Br$ (RT), and CuI-coated $CsPbI_2Br$ heated at 160°C

Sample	A_1	τ_1 (ns)	A_2	τ_2 (ns)	τ (ns)
Pure $CsPbI_2Br$	0.17	0.94	0.83	6.83	6.67
CuI-coated $CsPbI_2Br$ (RT)	0.81	0.44	0.19	5.62	4.32
CuI-coated $CsPbI_2Br$ (160°C)	0.83	0.75	0.17	4.45	2.78

$CsPbI_2Br$ films heated at 160°C to investigate whether the chemical environments of the constituent elements of $CsPbI_2Br$ changed after CuI modification. As shown in Fig. 4c, negligible differences between the elements' binding energies were observed for the pure $CsPbI_2Br$ and CuI-coated $CsPbI_2Br$ (RT) samples. This result indicates that the chemical environment of $CsPbI_2Br$ was not changed after applying CuI without heating. In contrast, depositing CuI on $CsPbI_2Br$ and then heating at 160°C induced considerable shifts of the peaks corresponding to Br, Cs, and Pb. Therefore, coating with CuI and subsequent heating markedly altered the chemical environment of $CsPbI_2Br$, which is in accordance with the phase degradation of $CsPbI_2Br$ discussed in previous sections.

Considering that the CuI granular capping layer induces an α-to-δ phase transition in $CsPbI_2Br$, we decided to investigate the effect of the contact area between CuI and $CsPbI_2Br$ on this phase transition. Commercial CuI powder (equal amount to that of colloidal CuI) was dispersed in chlorobenzene (chlorobenzene does not dissolve CuI). Then, the commercial CuI suspension was spin coated on $CsPbI_2Br$ films, followed by annealing at 80, 120, 160, and 200°C, respectively. The films after annealing for 25 min are shown in Fig. 5a. The color change started at above 120°C. This behavior was similar to that of colloidal CuI-modified $CsPbI_2Br$, but the rate of the color change was slower. The UV-vis spectra of the commercial CuI-modified $CsPbI_2Br$ (Fig. 5b) showed that the intensity of the characteristic α-phase absorption of the device heated at 80°C coincided with that of pure α-$CsPbI_2Br$, in contrast to the obvious change for colloidal CuI-modified $CsPbI_2Br$. The XRD patterns in

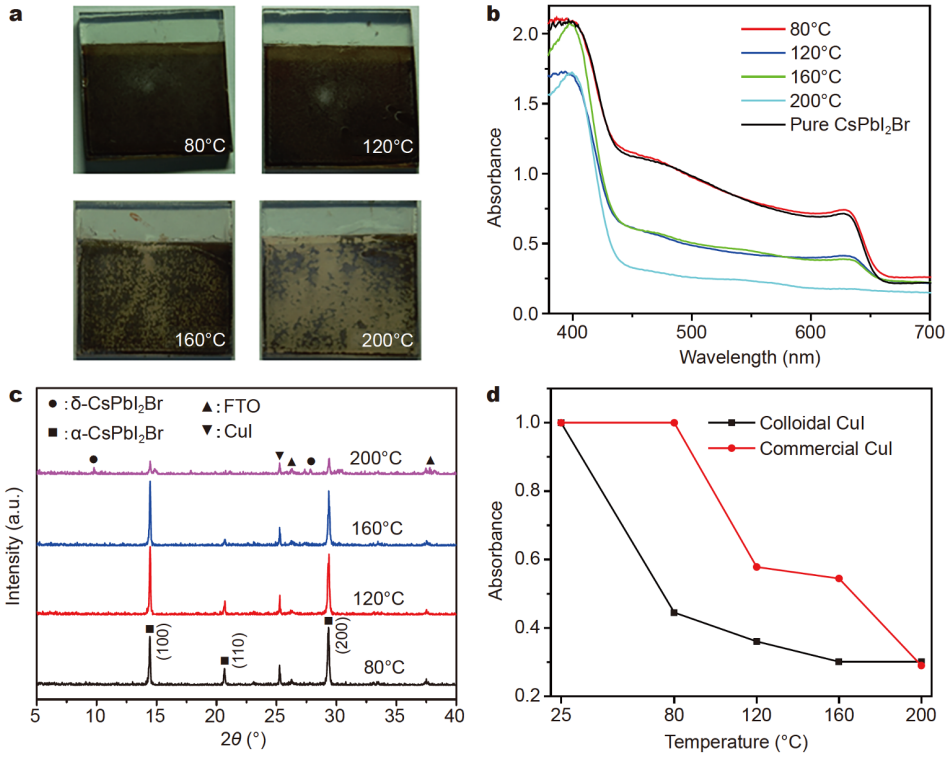

Figure 5 (a) Photographs, (b) UV-vis spectra, and (c) XRD patterns of the $CsPbI_2Br$ films covered with commercial CuI powder (equivalent to colloidal CuI) and heated at different temperatures for 25 min. (d) Normalized light absorption intensity at 628 nm of the $CsPbI_2Br$ films covered with CuI colloidal particles and commercial CuI powder heated at different temperatures.

Fig. 5c further confirmed the delay of the phase transition of $CsPbI_2Br$ when commercial CuI powder was used instead of colloidal CuI. The absorption intensity changes of $CsPbI_2Br$ at 628 nm when coated with commercial and colloidal CuI and heated at different temperatures were quantitatively measured, as shown in Fig. 5d. The results indicated that the CuI-induced phase degradation of $CsPbI_2Br$ is closely related with the contact area between CuI and $CsPbI_2Br$. The SEM images in Fig. 6 show that colloidal CuI particles have a much larger contact area with $CsPbI_2Br$ than that of commercial CuI. Elemental mapping of the $CsPbI_2Br$ films covered with colloidal and commercial CuI was conducted by using EDS to examine the presence and distribution of CuI, as shown in Fig. S2. The yellow areas in the EDS mapping images correspond to Cu, which coincided with the white dots in the SEM images. Fig. 7 presents a schematic of the phase degradation of $CsPbI_2Br$ films covered with commercial CuI (low coverage) and colloidal CuI (high coverage) during heating under the same conditions.

The change of CuI during heat treatment was also monitored using XRD and SEM measurements. XRD patterns (Fig. S3) indicated that the crystallinity of CuI increased markedly with rising temperature. SEM images of CuI colloidal particles and commercial CuI powder layers heated at different temperatures are shown in Figs S4 and S5, respectively. In addition to large particles, numerous small particles formed aggregates that became visible in the SEM images, as shown by the white dots in Fig. S5.

The phase transitions of $CsPbI_2Br$ and $CsPbI_3$ induced by moisture have been discussed previously [15,49,50]. It has been verified that water is adsorbed on the surface of the perovskite rather than penetrating into the crystal lattice. The adsorbed water molecules lead to the formation of halide vacancies near the surfaces of $CsPbI_2Br$ and $CsPbI_3$, which lower the nucleation free energy barrier and lead to the phase transition. Because α-$CsPbI_2Br$ is a metastable phase at RT, the kinetic energy barrier of its phase transition is relatively low. Once the halide vacancies form in the presence of moisture, the phase transition of α-$CsPbI_2Br$ accelerates. As CuI crystallizes during the heating process (moisture-free), we suspect that CuI particles interact with the underlying $CsPbI_2Br$ film and form chemical bonds. These chemical bonds between CuI and $CsPbI_2Br$ may lower the phase transition barrier, and the phase transition of $CsPbI_2Br$ accelerates upon heating. Therefore, our proposed CuI-induced phase transition process is different from the mechanism of the water-induced phase transition of

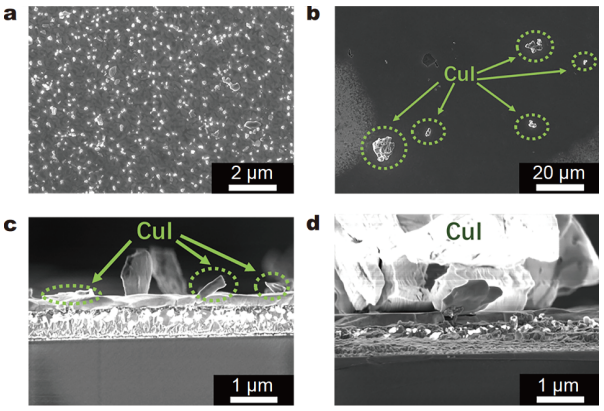

Figure 6 SEM images of (a) CuI colloidal particles and (b) a commercial CuI powder layer. Cross-sectional SEM images of FTO/TiO_2/$CsPbI_2Br$/CuI devices prepared with (c) CuI colloidal particles and (d) commercial CuI powder.

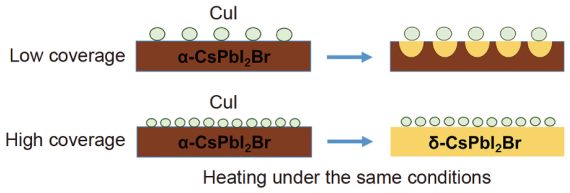

Figure 7 Schematic of the phase degradation of the $CsPbI_2Br$ films covered with commercial CuI (low coverage) and colloidal CuI (high coverage) induced by heating under the same conditions.

$CsPbI_2Br$, because it does not involve the formation of halide vacancies. The larger the contact area between CuI and $CsPbI_2Br$, the faster the phase transition. A proposed phase degradation process of $CsPbI_2Br$ induced by the CuI granular capping layer is shown in Fig. 8. However, further study is needed to elucidate the detailed mechanism of the CuI-induced phase transition of $CsPbI_2Br$.

CONCLUSIONS

The deposition of a CuI granular capping layer on a $CsPbI_2Br$ film followed by heating resulted in the degradation of the photoactive α phase $CsPbI_2Br$ to the non-perovskite δ phase. By removing moisture and solvents from CuI, it was confirmed that this phase degradation was caused by the CuI granular capping layer. The rate and extent of the phase degradation depended on the heating temperature and contact area between CuI and $CsPbI_2Br$. It is suspected that upon the crystallization of CuI, chemical bonds formed between CuI and $CsPbI_2Br$, which triggered the phase degradation during heat treatment. This mechanism is different from the widely recognized water-induced phase degradation of

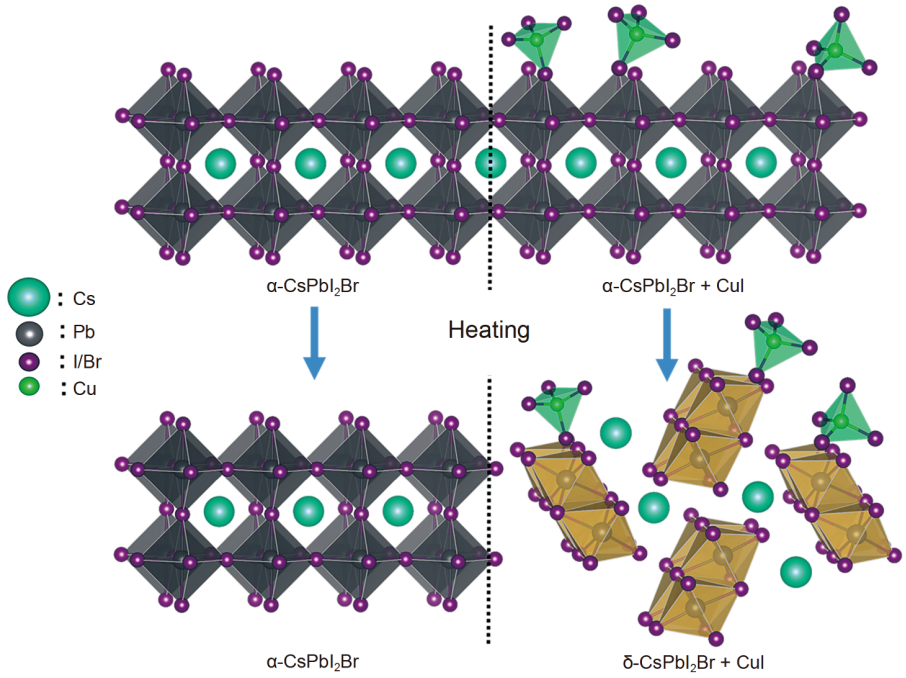

Figure 8 Schematic of the proposed $CsPbI_2Br$ phase degradation process induced by the CuI granular capping layer.

α-$CsPbI_2Br$. Our study indicates that attention should be paid to the interaction between the HTL and light-absorbing layer in PSCs. We should be cautious in the selection of inorganic HTM used with I-rich $CsPbX_3$ (X= Br, I) perovskites in high-performance optoelectronic devices.

Received 19 January 2020; accepted 10 July 2020; published online 2 September 2020

1 Ye Q, Zhao Y, Mu S, *et al.* Cesium lead inorganic solar cell with efficiency beyond 18% *via* reduced charge recombination. Adv Mater, 2019, 31: 1905143
2 Zhang J, Hodes G, Jin Z, *et al.* All-inorganic $CsPbX_3$ perovskite solar cells: progress and prospects. Angew Chem Int Ed, 2019, 58: 15596–15618
3 Chen H, Xiang S, Li W, *et al.* Inorganic perovskite solar cells: A rapidly growing field. Sol RRL, 2018, 2: 1700188
4 Du B, Xia Y, Wei Q, *et al.* All-inorganic perovskite nanocrystals-based light emitting diodes and solar cells. ChemNanoMat, 2018, 5: 266–277
5 Ye F, Yang W, Luo D, *et al.* Applications of cesium in the perovskite solar cells. J Semicond, 2017, 38: 011003
6 Tai Q, Tang KC, Yan F. Recent progress of inorganic perovskite solar cells. Energy Environ Sci, 2019, 12: 2375–2405
7 Zeng Q, Zhang X, Liu C, *et al.* Inorganic $CsPbI_2Br$ perovskite solar cells: the progress and perspective. Sol RRL, 2019, 3: 1800239
8 Zhang J, Jin Z, Liang L, *et al.* Iodine-optimized interface for inorganic $CsPbI_2Br$ perovskite solar cell to attain high stabilized efficiency exceeding 14%. Adv Sci, 2018, 5: 1801123
9 Tian J, Xue Q, Tang X, *et al.* Dual interfacial design for efficient $CsPbI_2Br$ perovskite solar cells with improved photostability. Adv Mater, 2019, 31: 1901152
10 Ma Q, Huang S, Chen S, *et al.* The effect of stoichiometry on the stability of inorganic cesium lead mixed-halide perovskites solar cells. J Phys Chem C, 2017, 121: 19642–19649
11 Liu C, Li W, Zhang C, *et al.* All-inorganic $CsPbI_2Br$ perovskite solar cells with high efficiency exceeding 13%. J Am Chem Soc, 2018, 140: 3825–3828
12 Bai D, Bian H, Jin Z, *et al.* Temperature-assisted crystallization for inorganic $CsPbI_2Br$ perovskite solar cells to attain high stabilized efficiency 14.81%. Nano Energy, 2018, 52: 408–415
13 Zhou W, Zhao Y, Zhou X, *et al.* Light-independent ionic transport in inorganic perovskite and ultrastable Cs-based perovskite solar cells. J Phys Chem Lett, 2017, 8: 4122–4128
14 Sutton RJ, Eperon GE, Miranda L, *et al.* Bandgap-tunable cesium lead halide perovskites with high thermal stability for efficient solar cells. Adv Energy Mater, 2016, 6: 1502458
15 Mariotti S, Hutter OS, Phillips LJ, *et al.* Stability and performance of $CsPbI_2Br$ thin films and solar cell devices. ACS Appl Mater Interfaces, 2018, 10: 3750–3760
16 Li Y, Wang Y, Zhang T, *et al.* Li dopant induces moisture sensitive phase degradation of an all-inorganic $CsPbI_2Br$ perovskite. Chem Commun, 2018, 54: 9809–9812
17 Zhang S, Wu S, Chen W, *et al.* Solvent engineering for efficient inverted perovskite solar cells based on inorganic $CsPbI_2Br$ light absorber. Mater Today Energy, 2018, 8: 125–133
18 Wang G, Liu J, Chen K, *et al.* High-performance carbon electrode-based $CsPbI_2Br$ inorganic perovskite solar cell based on poly(3-hexylthiophene)-carbon nanotubes composite hole-transporting layer. J Colloid Interface Sci, 2019, 555: 180–186
19 Liu C, Zhou X, Chen S, *et al.* Hydrophobic Cu_2O quantum dots enabled by surfactant modification as top hole-transport materials

for efficient perovskite solar cells. Adv Sci, 2019, 6: 1801169
20 Habisreutinger SN, Leijtens T, Eperon GE, *et al.* Carbon nanotube/polymer composites as a highly stable hole collection layer in perovskite solar cells. Nano Lett, 2014, 14: 5561–5568
21 Liao HC, Tam TLD, Guo P, *et al.* Dopant-free hole transporting polymers for high efficiency, environmentally stable perovskite solar cells. Adv Energy Mater, 2016, 6: 1600502
22 Guo X, Li J, Wang B, *et al.* Improving and stabilizing perovskite solar cells with incorporation of graphene in the spiro-OMeTAD layer: Suppressed Li ions migration and improved charge extraction. ACS Appl Energy Mater, 2020, 3: 970–976
23 Yin X, Zhou J, Song Z, *et al.* Dithieno[3,2-b:2′,3′-d]pyrrol-cored hole transport material enabling over 21% efficiency dopant-free perovskite solar cells. Adv Funct Mater, 2019, 29: 1904300
24 Yu Z, Sun L. Inorganic hole-transporting materials for perovskite solar cells. Small Methods, 2018, 2: 1700280
25 Chen J, Park NG. Inorganic hole transporting materials for stable and high efficiency perovskite solar cells. J Phys Chem C, 2018, 122: 14039–14063
26 Kung P, Li M, Lin P, *et al.* A review of inorganic hole transport materials for perovskite solar cells. Adv Mater Interfaces, 2018, 5: 1800882
27 Wu Z, Sun B. Constructing robust all-inorganic contacts enable stable perovskite solar cells with efficiencies over 20%. Sci China Mater, 2017, 61: 125–126
28 Chen Y, Yang Z, Wang S, *et al.* Design of an inorganic mesoporous holetransporting layer for highly efficient and stable inverted perovskite solar cells. Adv Mater, 2018, 30: 1805660
29 Gil B, Yun AJ, Lee Y, *et al.* Recent progress in inorganic hole transport materials for efficient and stable perovskite solar cells. Electron Mater Lett, 2019, 15: 505–524
30 Inudo S, Miyake M, Hirato T. Electrical properties of CuI films prepared by spin coating. Phys Status Solidi A, 2013, 210: 2395–2398
31 Uthayaraj S, Karunarathne D, Kumara G, *et al.* Powder pressed cuprous iodide (CuI) as a hole transporting material for perovskite solar cells. Materials, 2019, 12: 2037
32 Sepalage GA, Meyer S, Pascoe A, *et al.* Copper(I) iodide as hole-conductor in planar perovskite solar cells: probing the origin of *J-V* hysteresis. Adv Funct Mater, 2015, 25: 5650–5661
33 Chen D, Wang Y, Lin Z, *et al.* Growth strategy and physical properties of the high mobility p-type CuI crystal. Cryst Growth Des, 2010, 10: 2057–2060
34 Chen WY, Deng LL, Dai SM, *et al.* Low-cost solution-processed copper iodide as an alternative to PEDOT:PSS hole transport layer for efficient and stable inverted planar heterojunction perovskite solar cells. J Mater Chem A, 2015, 3: 19353–19359
35 Sun W, Ye S, Rao H, *et al.* Room-temperature and solution-processed copper iodide as the hole transport layer for inverted planar perovskite solar cells. Nanoscale, 2016, 8: 15954–15960
36 Haider SZ, Anwar H, Wang M. A comprehensive device modelling of perovskite solar cell with inorganic copper iodide as hole transport material. Semicond Sci Technol, 2018, 33: 035001
37 Wang H, Yu Z, Jiang X, *et al.* Efficient and stable inverted planar perovskite solar cells employing CuI as hole-transporting layer prepared by solid-gas transformation. Energy Technol, 2017, 5: 1836–1843
38 Yi Y, Zhu W, Li F, *et al.* Spontaneous configurational evolution induced by an *in situ* self-formed p-type CuI interface layer in perovskite solar cells. RSC Adv, 2016, 6: 82759–82762
39 Alhalib A, Moran WJ. CuI-catalyzed cycloisomerization of propargyl amides. Org Biomol Chem, 2014, 12: 795–800
40 Gharibzadeh S, Nejand BA, Moshaii A, *et al.* Two-step physical deposition of a compact CuI hole-transport layer and the formation of an interfacial species in perovskite solar cells. ChemSusChem, 2016, 9: 1929–1937
41 Gupta N, Dalvi A, Awasthi AM, *et al.* Electrical transport and crystallization in Cu^{+} ion substituted $AgI–Ag_2O–V_2O_5$ glassy superionic system. Solid State Ion, 2010, 180: 1607–1612
42 Li X, Wan M. Morphology and hydrophobicity of micro/nano-scaled cuprous iodide crystal. Cryst Growth Des, 2006, 6: 2661–2666
43 Christians JA, Fung RCM, Kamat PV. An inorganic hole conductor for organo-lead halide perovskite solar cells. Improved hole conductivity with copper iodide. J Am Chem Soc, 2014, 136: 758–764
44 Yin LQ, Peng JB. Hole transport in polymer P3HT with different annealing temperatures. Acta Phys Sin, 2009, 58: 3456–3460
45 Albert JNL, Young WS, Lewis Iii RL, *et al.* Systematic study on the effect of solvent removal rate on the morphology of solvent vapor annealed ABA triblock copolymer thin films. ACS Nano, 2012, 6: 459–466
46 Qin SM. Effect of rapid thermal annealing on property of nano-SnO_2thin film. J Infrared Millimeter Waves, 2008, 27: 101–104
47 Yang X, Loos J, Veenstra SC, *et al.* Nanoscale morphology of high-performance polymer solar cells. Nano Lett, 2005, 5: 579–583
48 Ma W, Yang C, Gong X, *et al.* Thermally stable, efficient polymer solar cells with nanoscale control of the interpenetrating network morphology. Adv Funct Mater, 2005, 15: 1617–1622
49 Dastidar S, Egger DA, Tan LZ, *et al.* High chloride doping levels stabilize the perovskite phase of cesium lead iodide. Nano Lett, 2016, 16: 3563–3570
50 Lin J, Lai M, Dou L, *et al.* Thermochromic halide perovskite solar cells. Nat Mater, 2018, 17: 261–267

Acknowledgements This work was supported primarily by the National Key Research and Development Program of China (2018YFA0209303), the National Natural Science Foundation of China (U1663228, 51902153, 51972165 and 61377051), and the Fundamental Research Funds for the Central Universities of China. We thank Prof. Wang X, Feng S, Huang H and Meng Q at the School of Physics, Nanjing University for informative discussions as well as experimental and technical assistance.

Author contributions Zhu Z conducted the experiments and wrote the paper. Yu T, Zhu Z, Feng J, and Li J conceived the experiments, analyzed the results, and revised the paper. Su W, Han X, Li Z, and Zou Z helped with sample preparation and characterization. All authors contributed to the general discussion.

Conflict of interest The authors declare that they have no conflict of interest.

Supplementary information Supporting data are available in the online version of the paper.

Zhi Zhu is a PhD student at the School of Physics, Nanjing University. He received his BSc degree from Wuhan University in 2017. His current research interest focuses on all-inorganic perovskites and hole-transporting materials in perovskite solar cells.

Tao Yu is a professor of physics at Nanjing University and Senior Scientist at the National Laboratory of Solid State Microstructures. He received his BSc and MSc degrees from Wuhan University in 1990 and 1993, respectively, and his PhD from Nanjing University in 1997. He worked as a visiting scholar & participating guest researcher in Prof. Yuen-Ron Shen's group at Lawrence Berkeley National Laboratory, UC Berkeley, USA, as part of the Berkeley Scholars' Program in 2002–2004. His research is focused on advanced functional micro/nanostructured materials that display photoelectric transformations as well as their solar photon conversion applications in the fields of clean and renewable energy.

Zhigang Zou received his PhD from the University of Tokyo, Japan, in 1996, and then he became a researcher at the Photoreaction Control Research Center, National Institute of Advanced Industrial Science and Technology (AIST), Japan. He has been with Nanjing University as a distinguished Professor of the Chang Jiang Scholars Program since 2003. He was elected as an academician of the Chinese Academy of Sciences in 2015. He is a director of Jiangsu Key Laboratory for Nano Technology, Nanjing University. His current research interests are photocatalysis, solar cells, and fuel cells.

由p型CuI颗粒覆盖层诱发的全无机$CsPbI_2Br$钙钛矿薄膜的相变研究

朱沿[1,2], 苏文婧[1,2], 冯建勇[1,3,4,5], 李金城[1,2], 韩晓鹏[1,2], 于涛[1,2,3,4*], 李朝升[1,3,4,5], 邹志刚[1,2,3,4]

摘要 由于具有良好的光吸收特性和光热稳定性, 富碘型全无机钙钛矿结构$CsPbI_2Br$光电功能材料受到了广泛关注. 然而, 具有钙钛矿结构的α相$CsPbI_2Br$在高湿度环境下易发生相变, 转变为具有非钙钛矿结构的δ相$CsPbI_2Br$. 因此基于$CsPbI_2Br$材料的光电器件通常需要在干燥环境中保存以维持器件性能稳定. 在本研究中, 我们将干燥且不吸湿的p型无机空穴传输材料CuI的颗粒涂覆在α相$CsPbI_2Br$薄膜表面并对样品进行加热, 实验测试结果表明, 这层CuI颗粒同样会诱发α相$CsPbI_2Br$转变为δ相$CsPbI_2Br$, 且该相变过程的速率随加热温度的升高、CuI颗粒覆盖度的提升而加快. 这种异于湿度诱导的钙钛矿结构$CsPbI_2Br$相变行为, 为研究者在思考、评估和分析基于富碘型全无机钙钛矿结构$CsPbX_3$ (X=Br, I)光电功能材料的高性能光电器件稳定性问题上, 提供了有益的借鉴和帮助.

